

**Numerical and Analytical
Spatial Coupling of a Lattice
Boltzmann Model and a Partial
Differential Equation**

Pieter Van Leemput

Wim Vanroose

Dirk Roose

Report TW 445, December 2005



Katholieke Universiteit Leuven
Department of Computer Science
Celestijnenlaan 200A – B-3001 Heverlee (Belgium)

Numerical and Analytical Spatial Coupling of a Lattice Boltzmann Model and a Partial Differential Equation

Pieter Van Leemput

Wim Vanroose

Dirk Roose

Report TW445, December 2005

Department of Computer Science, K.U.Leuven

Abstract

This article is concerned with the spatial coupling of a lattice Boltzmann model (LBM) and the finite difference discretization of the corresponding partial differential equation (PDE). At the interface, we have a one-to-many problem since the macroscopic PDE variables have to be mapped to more LBM variables. We show how this mapping can be done either analytically, using results from the Chapman-Enskog expansion or numerically, using a fixed point iterative scheme. The results are illustrated for different diffusive systems on a one-dimensional domain.

Keywords : spatial coupling, lattice Boltzmann model, constrained runs, hybrid model.

Numerical and Analytical Spatial Coupling of a Lattice Boltzmann Model and a Partial Differential Equation

Pieter Van Leemput, Wim Vanroose, and Dirk Roose

Department of Computer Science, Katholieke Universiteit Leuven,
Celestijnenlaan 200A, B-3001 Heverlee, Belgium
{pieter.vanleemput, wim.vanroose, dirk.roose}@cs.kuleuven.be

Summary. This article is concerned with the spatial coupling of a lattice Boltzmann model (LBM) and the finite difference discretization of the corresponding partial differential equation (PDE). At the interface, we have a one-to-many problem since the macroscopic PDE variables have to be mapped to more LBM variables. We show how this mapping can be done either analytically, using results from the Chapman-Enskog expansion or numerically, using a fixed point iterative scheme. The results are illustrated for different diffusive systems on a one-dimensional domain.

Key words: spatial coupling, lattice Boltzmann model, constrained runs, hybrid model.

1 Introduction

A dynamical system can be described by various models, each operating on a different level of abstraction. On the macroscopic level, there are partial differential equations (PDEs) that describe the system's evolution in terms of a few macroscopic variables, like density, velocity, etc. On a finer level, there are mesoscopic or pseudo particle models, like lattice Boltzmann models (LBMs) that use idealized particle distribution functions on a regular grid to describe the system. On the truly microscopic level, one has molecular dynamics and kinetic Monte Carlo methods that model the interactions between particles individually.

The choice for a particular model depends on several criteria. Macroscopic-level models, like PDEs, typically have a small dimensional state space and in general allow large time steps during simulation. However, they often fail to describe the dynamics of complex systems. Mesoscopic models like LBMs on the other hand allow the incorporation of complex physics in a more bottom-up way than macroscopic models but typically require more variables and smaller time steps. Furthermore, they can treat irregular domain boundaries

in a natural way. Similar advantages apply to microscopic models, but simulation with these models can be very expensive and often becomes prohibitive. Finally, when modeling a system with a higher level model fails because it can not be written in terms of variables at that particular level of abstraction only, i.e. when the higher level model does not close, a lower level model describing the same physics in more detail should be used.

Sometimes, the level of detail required to model a physical system changes from region to region and different models have to be used on different parts of the domain. At the interface between the models, there will be a mismatch in the kind (and number) of variables used by the different models. There, the variables have to be mapped to one another. Many such *hybrid* models, which couple a microscopic particle method to a macroscopic continuum method, have already been well developed, see e.g. [2, 6, 10, 11, 12, 15] and references therein.

In this article, we will spatially couple a LBM and a PDE model describing the same diffusive system in different regions of space on a one-dimensional domain. The PDE is discretized using finite differences and has the particle density as the sole macroscopic variable. For this setup, the corresponding LBM has three times as much variables (the particle distribution functions). Since there are more LBM than PDE variables, we have a one-to-many problem at the interface where we have to map densities to distribution functions. The inverse mapping of distribution functions to densities is straightforward because density is defined as the sum of the distribution functions.

Albuquerque *et al.* [1] used the Chapman-Enskog expansion to write the missing distribution functions at the interface as a functional of the density variable only. We will use the same concept but a different implementation. For cases where these functionals are not available or difficult to obtain analytically, the constrained runs scheme developed by Gear and Kevrekidis [8, 7] can be used to obtain these functionals numerically. This scheme performs a series of short microscopic (here LBM) simulations and resets the lowest order velocity moment (density) to its initial value while leaving the higher order moments unchanged. Van Leemput *et al.* showed in [17] that the application of the scheme to the LBM discussed here, produces a numerical approximation of the Chapman-Enskog relations that is correct up to first order.

The work described in this article is a step in the development of efficient methods for the coupling of LBM and PDE models. In the discussion, we have made some simplifying assumptions, e.g. we used the same time step and grid spacing for both the PDE and LBM. Taking different time steps can further optimize the methods presented here.

This article is organized as follows. In Sect. 2, we discuss different LBMs and the corresponding PDEs. Section 3 describes the constrained runs scheme applied to diffusive LBM. The issues concerning the coupling of the LBM and PDE are discussed in Sect. 4. In Sect. 5 we present numerical results on a) the FitzHugh-Nagumo reaction-diffusion system, b) a pure diffusion example and c) a growth-diffusion example where the LBM reaction term depends on

both the density and the velocities of the particles. Section 6 summarizes the main conclusions.

2 Models for One-Dimensional Diffusive Systems

In Sect. 2.1, we describe the finite difference discretization of the partial differential equation for one-dimensional reaction-diffusion systems. In Sect. 2.2, we describe the corresponding lattice Boltzmann BGK model with a reaction term depending on density only. Section 2.3 shows that both models are equivalent when the macroscopic solution is smooth. In Sect. 2.4, we briefly describe a lattice Boltzmann BGK model with a velocity dependent reaction term to simulate growth-diffusion systems. The corresponding PDE is also given.

2.1 Partial Differential Equation (PDE)

In a one-dimensional reaction-diffusion system, the partial differential equation (PDE) describing the evolution of the particle density (concentration) $\rho(x, t)$ as a function of space x and time t is given by

$$\frac{\partial \rho(x, t)}{\partial t} = D \frac{\partial^2 \rho(x, t)}{\partial x^2} + F(\rho(x, t)) \quad (1)$$

where D is the diffusion coefficient and $F(\rho(x, t))$ a macroscopic reaction force term which depends on $\rho(x, t)$ only.

To find a solution of (1), the equation is discretized using finite differences (forward difference in time and central difference in space) to obtain

$$\begin{aligned} \rho(x, t + \Delta t) = & \rho(x, t) + \frac{\Delta t D}{\Delta x^2} (\rho(x + \Delta x, t) - 2\rho(x, t) + \rho(x - \Delta x, t)) \\ & + \Delta t F(\rho(x, t)) \end{aligned} \quad (2)$$

with Δx and Δt the corresponding space and time steps.

2.2 Lattice Boltzmann Model (LBM)

Boltzmann models describe the evolution of a distribution function $f(x, v, t)$ that represents the number of particles that move with certain velocity v at position x and time t . Lattice Boltzmann models (LBM) [3, 13] use discretized distribution functions $f_i(x, t)$ with velocity v_i that are defined on a space-time lattice with grid spacing Δx in space and Δt in time. On a one-dimensional domain, only three values are considered for the velocity (D1Q3 model):

$$v_i = c_i \frac{\Delta x}{\Delta t}, \quad c_i = i \in \{-1, 0, 1\} \quad (3)$$

with c_i the dimensionless lattice velocity.

The lattice Boltzmann evolution law for the distribution functions is

$$f_i(x + c_i \Delta x, t + \Delta t) = (1 - \omega) f_i(x, t) + \omega f_i^{eq}(x, t) + R_i(x, t) \quad (4)$$

for $i \in \{-1, 0, 1\}$. The right hand side of (4) updates the values $f_i(x, t)$ to *post-collision* values $f_i^*(x, t^*)$ (with $t < t^* < t + \Delta t$). Afterwards, these values propagate to a neighboring lattice site according to their velocity direction (left hand side of (4)). Diffusive collisions are modeled by the Bhatnagar-Gross-Krook (BGK) collision term $-\omega(f_i(x, t) - f_i^{eq}(x, t))$ in (4) as a relaxation to a *local diffusive equilibrium*

$$f_i^{eq}(x, t) = \frac{1}{3} \rho(x, t). \quad (5)$$

The BGK relaxation coefficient ω in (4) will be defined in Sect. 2.3. Reactions are modelled by the term $R_i(x, t)$ in (4) as [14, 5]

$$R_i(x, t) = \frac{\Delta t}{3} F(\rho(x, t)) \quad (6)$$

with $F(\rho(x, t))$ defined in (1). Here, it is assumed that reactions occur at the local diffusive equilibrium [4].

The particle density $\rho(x, t)$, i.e. the macroscopic variable (cf. (1)), is defined as the zeroth order velocity moment of the distribution functions

$$\rho(x, t) = \sum_{i=-1}^1 f_i(x, t) = \sum_{i=-1}^1 f_i^{eq}(x, t), \quad (7)$$

where the second equality expresses that the BGK diffusive collisions locally conserve density (compare (5)).

In a similar way, we define the dimensionless first and second order velocity moments (up to the factor 1/2 for the second order moment) as

$$\phi(x, t) = \sum_{i=-1}^1 c_i f_i(x, t) \quad \xi(x, t) = \frac{1}{2} \sum_{i=-1}^1 c_i^2 f_i(x, t) \quad (8)$$

We will refer to these moments as the “momentum” ϕ and (kinetic) “energy” ξ (although these are non-conserved quantities in a diffusive system). The state of the LBM at time t and position x is then fully determined by either the distribution functions $\mathbf{f} = [f_{-1} \ f_0 \ f_1]'$ or the moments $\boldsymbol{\varrho} = [\rho \ \phi \ \xi]'$. By definition,

$$\begin{bmatrix} \rho \\ \phi \\ \xi \end{bmatrix} = \begin{bmatrix} 1 & 1 & 1 \\ -1 & 0 & 1 \\ \frac{1}{2} & 0 & \frac{1}{2} \end{bmatrix} \begin{bmatrix} f_{-1} \\ f_0 \\ f_1 \end{bmatrix} \Leftrightarrow \boldsymbol{\varrho} = M \mathbf{f} \quad (9)$$

and vice versa $\mathbf{f} = M^{-1} \boldsymbol{\varrho}$ (one-to-one relationship).

2.3 Relations between LBM and PDE

When the solution of the LBM varies slowly on a macroscopic length and time scale, we can show that the LBM from Sect. 2.2 reduces to the PDE introduced in Sect. 2.1 using a multiscale Chapman-Enskog expansion [3]. Under this condition, both models describe the same macroscopic behavior. To this end, we define a small tracer parameter ϵ and the scaling $x_\epsilon = \epsilon x$, $t_\epsilon = \epsilon^2 t$ such that

$$\frac{\partial}{\partial x} = \epsilon \frac{\partial}{\partial x_\epsilon} \quad \text{and} \quad \frac{\partial}{\partial t} = \epsilon^2 \frac{\partial}{\partial t_\epsilon}. \quad (10)$$

For reaction-diffusion problems, we further assume that the reaction term $R_i(x, t)$ in (4) is of second order, i.e. $R_i = \epsilon^2 R_{i, \epsilon}$ [3, 5], which explains the choice in (6).

A second order Taylor expansion of the term $f_i(x + c_i \Delta x, t + \Delta t)$ in (4) around $f_i(x, t)$ leads to

$$\begin{aligned} c_i \Delta x \frac{\partial f_i}{\partial x} + \Delta t \frac{\partial f_i}{\partial t} + \frac{c_i^2 \Delta x^2}{2} \frac{\partial^2 f_i}{\partial x^2} + c_i \Delta x \Delta t \frac{\partial^2 f_i}{\partial x \partial t} + \frac{\Delta t^2}{2} \frac{\partial^2 f_i}{\partial t^2} \\ = -\omega(f_i - f_i^{eq}) + R_i \end{aligned} \quad (11)$$

Introducing the tracer scaling (10) and dropping the subscript ϵ notation, we obtain

$$\begin{aligned} \epsilon c_i \Delta x \frac{\partial f_i}{\partial x} + \epsilon^2 \Delta t \frac{\partial f_i}{\partial t} + \epsilon^2 \frac{c_i^2 \Delta x^2}{2} \frac{\partial^2 f_i}{\partial x^2} + \epsilon^3 c_i \Delta x \Delta t \frac{\partial^2 f_i}{\partial x \partial t} + \epsilon^4 \frac{\Delta t^2}{2} \frac{\partial^2 f_i}{\partial t^2} \\ = -\omega(f_i - f_i^{eq}) + \epsilon^2 R_i \end{aligned} \quad (12)$$

The distribution functions $f_i(x, t)$ are expanded in terms of increasingly higher order contributions $f_i^{[0]}$, $f_i^{[1]}$, \dots as follows

$$f_i = f_i^{[0]} + \epsilon f_i^{[1]} + \epsilon^2 f_i^{[2]} + \dots \quad (13)$$

We substitute (13) in (12) and keep only terms up to second order to obtain

$$\begin{aligned} \epsilon c_i \Delta x \frac{\partial f_i^{[0]}}{\partial x} + \epsilon^2 c_i \Delta x \frac{\partial f_i^{[1]}}{\partial x} + \epsilon^2 \Delta t \frac{\partial f_i^{[0]}}{\partial t} + \epsilon^2 \frac{c_i^2 \Delta x^2}{2} \frac{\partial^2 f_i^{[0]}}{\partial x^2} \\ = -\omega(f_i^{[0]} + \epsilon f_i^{[1]} + \epsilon^2 f_i^{[2]} - f_i^{eq}) + \epsilon^2 R_i \end{aligned} \quad (14)$$

This equation should hold for each order separately. Equating the zeroth order terms leads to

$$f_i^{[0]} = f_i^{eq} = \frac{1}{3} \rho \quad (15)$$

The part of order ϵ leads to the following expression for the first order correction $f_i^{[1]}(x, t)$

$$f_i^{[1]} = -\frac{c_i \Delta x}{\omega} \frac{\partial f_i^{[0]}}{\partial x} = -\frac{c_i \Delta x}{3\omega} \frac{\partial \rho}{\partial x}, \quad (16)$$

Gathering the terms of order ϵ^2 in (14), we have

$$c_i \Delta x \frac{\partial f_i^{[1]}}{\partial x} + \frac{c_i^2 \Delta x^2}{2} \frac{\partial^2 f_i^{[0]}}{\partial x^2} + \Delta t \frac{\partial f_i^{[0]}}{\partial t} = -\omega f_i^{[2]} + R_i \quad (17)$$

Substitution of (15), (16) and (6) results in the following expression for the second order contribution $f_i^{[2]}(x, t)$

$$f_i^{[2]} = -\frac{c_i^2 \Delta x^2}{6\omega^2} (\omega - 2) \frac{\partial^2 \rho}{\partial x^2} + \frac{\Delta t}{3\omega} \left(F(\rho) - \frac{\partial \rho}{\partial t} \right) \quad (18)$$

When we sum (18) over all velocities, we obtain

$$\frac{\partial \rho}{\partial t} = -\frac{\Delta x^2}{3\omega \Delta t} (\omega - 2) \frac{\partial^2 \rho}{\partial x^2} + F(\rho) \quad (19)$$

where we used the fact that $\sum_i f_i^{[2]} = 0$ (sum up (13) and use (7)). Comparing (19) to (1), we obtain the relation between D and ω (cf. [14])

$$\omega = \frac{2}{1 + 3D \frac{\Delta t}{\Delta x^2}}. \quad (20)$$

Expansion (13) together with (15), (16) and (18) can be used to represent the state of the LBM system. Note that, since we dropped the index ϵ notation in the derivation, the actual macroscopic derivatives are obtained by combining (10) with (13). Using (9), the equivalent higher order moments $\phi(x, t)$ and $\xi(x, t)$ can be computed as functionals of the density $\rho(x, t)$ only

$$\begin{aligned} \phi &= -\frac{2\Delta x}{3\omega} \frac{\partial \rho}{\partial x} + O(\epsilon^3), \\ \xi &= \frac{\rho}{3} - \frac{\Delta t}{6\omega} \left(F(\rho) - \frac{\partial \rho}{\partial t} \right) + O(\epsilon^4). \end{aligned} \quad (21)$$

These functionals, and by extension (15), (16) and (18), are called *slaving relations*.

Note that, using the PDE (19) itself, (18) can be rewritten as

$$f_i^{[2]} = -\frac{\Delta t}{6\omega} (3c_i^2 - 2) \left(F(\rho) - \frac{\partial \rho}{\partial t} \right) = -\frac{\Delta x^2}{18\omega^2} (\omega - 2) (3c_i^2 - 2) \frac{\partial^2 \rho}{\partial x^2}. \quad (22)$$

2.4 Velocity Dependent Mesoscopic Reactions: Growth-Diffusion

Many microscopic systems have reaction rates that depend on the velocities of the colliding particles. One example is the ionization reaction that appears in electron transport through a molecular gas. During transport, the electrons collide with the molecules and transfer part of their energy. Fast electrons slow down by kicking additional electrons out of the molecule during reactive

collisions. Slow electrons collide elastically and only change their direction. This can only be modeled by a velocity dependent reaction term.

The LBM (4) in Sect. 2.2 is not suitable to describe such system because the reaction term (6) depends on the density only. However, the classical lattice Boltzmann BGK equation can be extended to include a more general velocity dependent reaction term

$$f_i(x+c_i\Delta x, t+\Delta t) - f_i(x, t) = -\omega(f_i(x, t) - f_i^{eq}(x, t)) + \Delta t \sum_j A_{ij} f_j(x, t). \quad (23)$$

At each time step, the rate A_{ij} denotes the chance that either a particle with speed c_j ends up with speed c_i or that a particle has been created or destroyed during the reaction. The microscopic velocities are again crudely discretized. As in Sect. 2.2, we implemented the D1Q3 model (3) on a one-dimensional domain.

In this article, we discuss a limited class of models with velocity dependent reaction rates. We specifically look at a problem that gives rise to a growth-diffusion PDE on a macroscopic scale when the solution of (23) is slowly varying. As described in [18], this reduced model can be derived through a Chapman-Enskog expansion similar to the one outlined in Sect. 2.2, and is given by

$$\frac{\partial \rho(x, t)}{\partial t} = D \frac{\partial^2 \rho(x, t)}{\partial x^2} + \alpha \rho(x, t), \quad (24)$$

where both D and the growth rate α depend on the microscopic reaction rates A_{ij} and relaxation parameter ω . As in Sect. 2.1, (24) can be discretized using finite differences.

3 Constrained Runs Scheme

Given only the density values on the domain, the full state of the LBM can be represented by the slaving relations (15), (16) and (18) as described in Sect. 2.3. Assuming that such relations are unavailable or difficult to obtain analytically, the *constrained runs scheme* [8, 7] can be used to approximate these relations numerically.

The application of the constrained runs scheme to the LBM from Sect. 2.2 or Sect. 2.4 is outlined in Algorithm 1. Given the initial density profile $\rho^{(0)}$, an initial guess for $f_i(x, t)$ is computed using e.g. (5). The LBM is then repeatedly used to evolve the state for a short time τ . After each such simulation the transformation (9) is used to reset the lowest moment of the distribution functions to the initial density profile.

The constrained runs scheme can be defined as a map

$$\boldsymbol{\varrho}^{(k+1)} = \mathcal{C}_\tau(\boldsymbol{\varrho}^{(k)}); \quad k = 0, 1, 2, \dots, K \quad (25)$$

on the state vector $\boldsymbol{\varrho}^{(k)} = [\rho^{(0)} \ \phi^{(k)} \ \xi^{(k)}]'$; with k the iteration number and τ the simulation time of the inner microscopic model, here the LBM. Since

Algorithm 1 Constrained runs scheme for a one-dimensional diffusive LBM

Required: $\rho^{(0)} = \rho(x, 0)$
 $f_i^{(0)} = w_i \rho^{(0)}$; $\sum_{i=-1}^1 w_i = 1$, e.g. $w_i = 1/3$ Choose $f_i^{(0)}$ s.t. (7) holds

repeat
 $\mathbf{f}^{(k+1)} = \text{LBM}(\mathbf{f}^{(k)})$ LBM simulation (4) over time τ
 $\mathbf{q}^{(k+1)} = M\mathbf{f}^{(k+1)}$ Corresponding $\phi^{(k+1)}$ and $\xi^{(k+1)}$ (9)
 $\rho^{(k+1)} = \rho^{(0)}$ Reset macroscopic variables
 $\mathbf{f}^{(k+1)} = M^{-1}\mathbf{q}^{(k+1)}$ Map back (9)

until convergence heuristic $< \theta$, with $\theta \ll 1$

$\rho^{(k+1)}$ is reset to $\rho^{(0)}$ after each step, the map effectively iterates on the higher order moments ϕ and ξ to obtain a fixed point.

A straightforward choice for the convergence heuristic in Algorithm 1 is

$$\|\phi^{(k+1)}(x) - \phi^{(k)}(x)\|_2 < \theta \quad \text{and} \quad \|\xi^{(k+1)}(x) - \xi^{(k)}(x)\|_2 < \theta \quad (26)$$

with θ a user-defined tolerance ($\theta \ll 1$). Figure 1 sketches the evolution of the procedure.

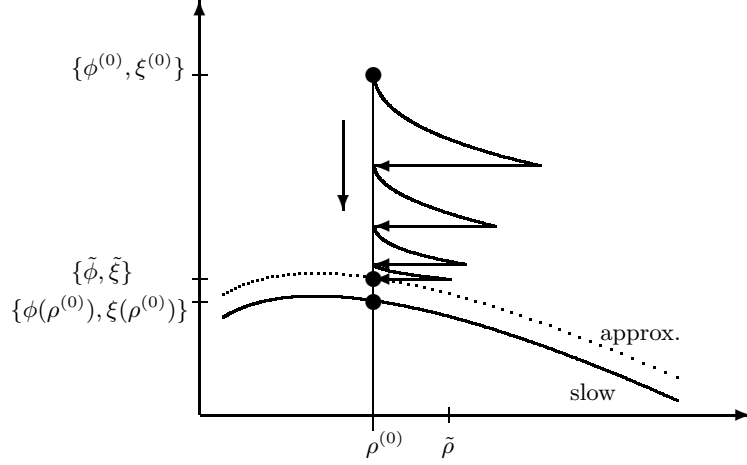


Fig. 1. Sketch of the evolution of the constrained runs scheme. The higher order moments ϕ and ξ are plotted with respect to the macroscopic variable ρ . The density ρ is reset to the given $\rho^{(0)}$ after each LBM simulation. The constrained runs scheme iterates towards a fixed point $\{\tilde{\phi}, \tilde{\xi}\}$ that is an “approximate” manifold $\{\phi(\rho^{(0)}), \xi(\rho^{(0)})\}$ (21). The fixed point lies on an “approximate” manifold while the exact solution lies on the slow manifold described by ρ . The value $\tilde{\rho}$ is the density corresponding to $\{\tilde{\phi}, \tilde{\xi}\}$ (before the final reset to $\rho^{(0)}$) and will be useful as an estimate for the error.

In [17] we analyzed the application of the constrained runs scheme for the initialization of the LBM for one-dimensional reaction-diffusion problems

(see Sect. 2.2). We have proven that the scheme is unconditionally stable and convergent. Below, we restate the main theorems.

Theorem 1 (Stability theorem). *The constrained runs scheme for the lattice Boltzmann BGK model that describes a one-dimensional reaction-diffusion system with either periodic, no-flux or Dirichlet boundary conditions (and with the reaction term depending on ρ only (6)), is unconditionally stable.*

Proof (Outline). The eigenvalues μ of the linearization (the Jacobian matrix) of one step of the fixed point iterator (25) determine the stability of Algorithm 1. If all eigenvalues in the spectrum $\sigma(\mathcal{C}_\tau)$ lie within the unit circle, i.e. $\forall \mu \in \sigma(\mathcal{C}_\tau) : |\mu| < 1$, the iteration is stable. For the three types of boundary conditions considered, we prove in [17] that these eigenvalues lie on a circle centered at the origin with radius $|1 - \omega|$. The constrained runs iteration is unconditionally stable because $0 < \omega < 2$ [13] (compare (20)) and thus always $|\mu| = |1 - \omega| < 1$.

Theorem 2 (Asymptotic convergence factor). *As a corollary of the above proof, the asymptotic convergence factor $\eta := \max\{|\mu| : \forall \mu \in \sigma(\mathcal{C}_\tau)\}$ is equal to $|1 - \omega|$.*

Theorem 3 (Convergence theorem). *The constrained runs algorithm for the LBM described in Theorem 1 converges to a first order correct approximation $\{\tilde{\phi}, \tilde{\xi}\}$ of the slaved state (21). The approximation error depends on $\tilde{\rho} - \rho^{(0)}$, where $\rho^{(0)}$ is the initial density and $\tilde{\rho}$ is the internal simulated-upon density corresponding to $\{\tilde{\phi}, \tilde{\xi}\}$ (before the final reset to $\rho^{(0)}$).*

The proof is quite technical and given in [17]. Using the one-to-one relationship between $\boldsymbol{\rho}$ and \mathbf{f} (9), the expressions for the constrained runs fixed point $\{(\rho^{(0)}), \tilde{\phi}, \tilde{\xi}\}$ from [17] can be written as follows

$$\tilde{f}_i = \frac{1}{3}\rho^{(0)} - \frac{c_i \Delta x}{3\omega} \frac{\partial \rho^{(0)}}{\partial x} - \frac{\Delta t}{6\omega} (3c_i^2 - 2) \left(F(\rho^{(0)}) - 3 \frac{(\tilde{\rho} - \rho^{(0)})}{\Delta t} \right). \quad (27)$$

When we compare this expression with the expansion of f_i (13) in its Chapman-Enskog components $f_i^{[0]}$, $f_i^{[1]}$ and $f_i^{[2]}$ (15)–(18), we see that (27) is indeed correct up to first order in the Chapman-Enskog expansion. Due to the approximation error (the third term) in (27), the fixed point \tilde{f}_i (or equivalently $\{\tilde{\phi}, \tilde{\xi}\}$) lies on an “approximate” manifold instead of the true slow manifold described by the macroscopic variable ρ (cf. Fig. 1). To make this error as small as possible, we choose $\tau = \Delta t$ (one LBM time step).

4 Spatial Coupling

4.1 Problem Specification

In this section, we describe how to couple the PDE and LBM from Sect. 2. In our setup, shown in Fig. 2, the one-dimensional domain is split into two

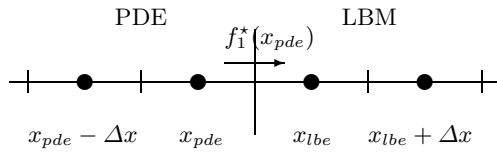


Fig. 2. Spatial coupling of a PDE (left) and LBM (right) on a one-dimensional domain. The interface lies in between two lattice sites. The evolution of the solution in the LBM region requires the propagating (post-collision) distribution value $f_1^*(x_{pde}, t^*)$ coming from the PDE domain. Since the PDE only evolves density values $\rho(x, t)$, this value is unavailable.

non-overlapping sublattices. Another option, using one overlapping lattice site is discussed in [1]. The PDE is applied to the left sublattice and the LBM to the right sublattice. We use the same lattice spacing Δx and time step Δt for both the PDE and LBM, i.e. the simplest coupled space-time lattice. Since the LBM is a mesoscopic model (as opposed to a truly microscopic model), using the same Δx is very reasonable. On the other hand, using the same Δt is an important simplification. More efficient coupling schemes, especially those that allow for different Δt , will be the subject of future research.

Since the PDE and LBM use a different set of variables, namely ρ versus $\mathbf{f} = [f_{-1} f_0 f_1]^T$, we have to be careful how to exchange information at the interface during time simulation. To evolve the PDE in x_{pde} , the value $\rho(x_{lbe}, t) = \rho(x_{pde} + \Delta x, t)$ (see Fig. 2) is needed in (2). This value is computed from the LBM variables $f_i(x_{lbe}, t)$ using (7).

The inverse problem, where we have to transfer information from the PDE to the LBM region is more difficult. To evolve the LBM (4) in x_{lbe} from t to $t + \Delta t$, we need to map a single density value onto three corresponding distributions. This is formally stated as

$$\rho(x_{pde}, t) \mapsto f_i(x_{pde}, t); \quad i \in \{-1, 0, 1\}. \quad (28)$$

Since (7) should hold, this leaves two degrees of freedom.

The initialization of a LBM from a given density profile as described in [17] faces the same one-to-many problem, but there the problem concerns the whole domain instead of a single lattice site.

We will use the analytical slaving relations (15) and (16) or the corresponding numerical approximation (27) by the constrained runs scheme to derive the distributions at the interface given only the value of $\rho(x_{pde}, t)$. In the next sections we discuss these two strategies.

4.2 Implementation using First Order Perturbations

In order to evolve the solution in the leftmost site x_{lbe} of the LBM sublattice, we need the value of the distribution function $f_1(x_{pde}, t)$ coming from the

PDE lattice that propagates into the LBM sublattice (see Fig. 2). This value is missing, but can be computed as follows.

The key observation is that the PDE (2) simulates “directly” from t to $t + \Delta t$, while the LBM (4) executes in two phases: first, collisions and reactions to go from t to t^* and secondly, propagation of the post-collision distributions f_i^* to get from t^* to $t + \Delta t$. Thus we actually need the post-collision value $f_1^*(x_{pde}, t^*)$ instead of the value $f_1(x_{pde}, t)$.

First, we compute the distribution $f_1(x_{pde}, t)$ corresponding to the PDE density $\rho(x_{pde}, t)$ at time t , using the first order perturbations (15) and (16)

$$\begin{aligned} f_1(x_{pde}, t) &= f_1^{[0]}(x_{pde}, t) + f_1^{[1]}(x_{pde}, t) \\ &= \frac{1}{3}\rho(x_{pde}, t) - \frac{\Delta x}{3\omega} \frac{\rho(x_{lbe}, t) - \rho(x_{pde} - \Delta x, t)}{2\Delta x} \end{aligned} \quad (29)$$

In (29), the derivative $\partial\rho(x_{pde}, t)/\partial x$ is approximated with central differences. The value $\rho(x_{lbe}, t)$ is obtained from the LBM domain using (7).

Afterwards, the corresponding post-collision value $f_1^*(x_{pde}, t^*)$ is computed from $f_1(x_{pde}, t)$ (29) using the LBM:

$$f_1^*(x_{pde}, t^*) = (1 - \omega)f_1(x_{pde}, t) + \frac{\omega}{3}\rho(x_{pde}, t) + \frac{\Delta t}{3}F(\rho(x_{pde}, t)) \quad (30)$$

Finally, it is this value that is propagated to x_{lbe} , i.e.

$$f_1(x_{lbe}, t + \Delta t) = f_1^*(x_{pde}, t^*) \quad (31)$$

Note that the outgoing post-collision value $f_{-1}^*(x_{lbe}, t^*)$ that enters the PDE domain is never used.

4.3 Implementation using Constrained Runs

As explained in Sect. 3, the numerical computation of $f_i(x, t)$ from a given $\rho(x, t)$ by the constrained runs scheme is accurate up to first order. As an alternative to the procedure from Sect. 4.2, we can thus replace (29) with Algorithm 1 and apply (30) and (31) to the result.

As already mentioned in Sect. 4.1, Algorithm 1 solves the one-to-many problem for the LBM on the full domain, whereas the mapping problem for spatial coupling (28) is an issue in a single lattice site x_{pde} only.

Since information in the (explicit) LBM (4) propagates over only one lattice site in each iteration, Algorithm 1 requires initial density values on a sublattice with at least $2K + 1$ lattice sites, symmetrically distributed around x_{pde} , with K the number of iterations needed for convergence of the algorithm. We can impose arbitrary boundary conditions on this sublattice because the boundary information will not have reached x_{pde} within K iterations.

Alternatively, one can drop the outer lattice sites (and distribution functions) during propagation in each iteration to obtain a *funneled* scheme. Here

we keep only the information streaming towards x_{pde} . Again it is important that there are at least $2K + 1$ initial sites, symmetrically positioned around x_{pde} . Note that this funneled scheme decreases the amount of work with a factor two. On the other hand, this implementation requires changes to the propagation step of the LBM in Algorithm 1, which may not be desirable.

Of course, for the above implementations to work, the number of constrained runs K has to be obtained first. To this end, one could do a preliminary run on (part of) the domain with Algorithm 1 and observe its convergence (see also [17]).

Depending on the implementation, the amount of work needed by the scheme is either K^2 or $K^2/2$. If K is large and the full domain is small, this is an expensive overhead since the scheme has to be used in between each time step Δt . Of course, for situations where the analytical slaving relations (29) are unknown or difficult to obtain analytically, it is the only alternative.

5 Numerical Results

5.1 FitzHugh-Nagumo Reaction-Diffusion System

We will apply the proposed coupled PDE/LBM method to the FitzHugh-Nagumo (FHN) reaction-diffusion system on a one-dimensional domain. For this problem, both the PDE and LBM are known and valid on the full domain. The system consists of two species: an activator and an inhibitor.

The PDE system describes the evolution of the activator $\rho^{ac}(x, t)$ and inhibitor $\rho^{in}(x, t)$ concentration (density) and is given by

$$\begin{cases} \frac{\partial \rho^{ac}}{\partial t} = D^{ac} \frac{\partial^2 \rho^{ac}}{\partial x^2} + \rho^{ac} - (\rho^{ac})^3 - \rho^{in} , \\ \frac{\partial \rho^{in}}{\partial t} = D^{in} \frac{\partial^2 \rho^{in}}{\partial x^2} + \varepsilon(\rho^{ac} - a_1 \rho^{in} - a_0) . \end{cases} \quad (32)$$

For each species, the LBM is described in Sect. 2.2. Given the PDE reaction terms in (32), the LBM reaction terms are defined as (6)

$$\begin{aligned} R_i^{ac}(x, t) &= \frac{\Delta t}{3} (\rho^{ac}(x, t) - (\rho^{ac})^3(x, t) - \rho^{in}(x, t)) , \\ R_i^{in}(x, t) &= \frac{\Delta t}{3} \varepsilon (\rho^{ac}(x, t) - a_1 \rho^{in}(x, t) - a_0) , \quad i \in \{-1, 0, 1\} . \end{aligned} \quad (33)$$

For our numerical tests, we choose the parameter values as $D^{ac} = 1$, $D^{in} = 4$, $a_0 = -0.03$, $a_1 = 2$ and $\varepsilon = 0.05$. The domain has length $L = 20$. At the boundaries of the domain, we impose homogeneous Neumann (or no-flux) boundary conditions which are implemented in the LBM using the halfway bounce-back scheme [9]. For both models, the lattice points x lie at the midpoints of 200 lattice intervals, such that $\Delta x = 0.1$. We choose the time step $\Delta t = 0.001$ [16].

5.2 Spatial Coupling of the FHN PDE and LBM

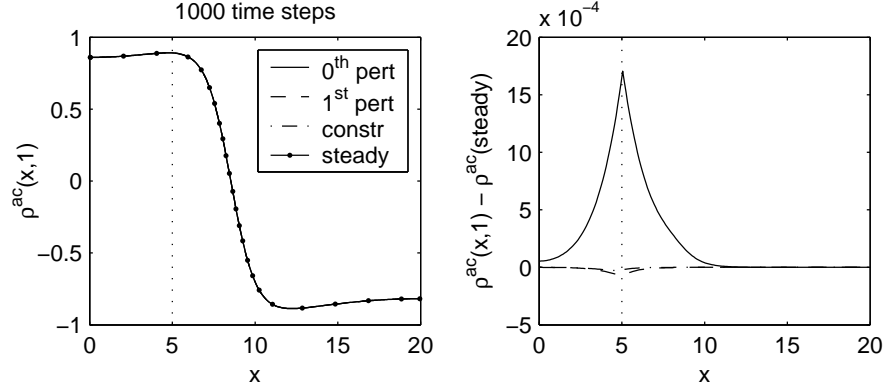


Fig. 3. Solution of the coupled FHN PDE/LBM model after 1000 time steps. We used either zeroth order perturbations (34), first order perturbations (Sect. 4.2) or constrained runs (Sect. 4.3) at the interface. The activator density $\rho^{ac}(x, t)$ at $t = 1000\Delta t$ is shown left and the difference with respect to the reference solution, the LBM steady state on the full domain, is shown right. The dotted line shows the position of the interface.

In this section, we spatially couple the FHN PDE (left) and FHN LBM (right) models from Sect. 5.1. The domain is divided as in Fig. 2 with the interface positioned at $x = 5$ (in between two lattice sites). Correspondingly, we solve predominately with the LBM. We initialize the coupled model with the LBM steady state computed on the full domain (see [16]). As described in Sect. 4, we use either first order perturbations or constrained runs at the interface. For our problem, the number of constrained iterations needed for convergence is $K = 25$ (see [17]).

As an illustration, we also compare our results with a modification of the scheme described in Sect. 4.2. We drop the spatial derivatives from (29) to obtain

$$f_1(x_{pde}, t) = f_1^{[0]}(x_{pde}, t) = \frac{1}{3}\rho(x_{pde}, t) \quad (34)$$

and replace (29) by (34). Afterwards, we proceed as in Sect. 4.2. We call this modification the zeroth order coupling scheme.

We first look at the short time behavior of the coupled problem. Figure 3 shows the results after 1000 time steps. On the time scale considered, the difference between the densities cannot be resolved visually. The corresponding error is shown in the right panel. Here, we see that the zeroth order coupling scheme results in a significant interfacial error, while the error with first order

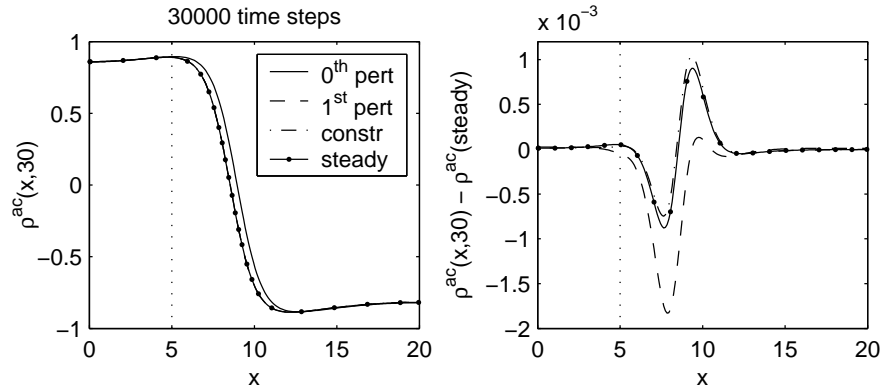


Fig. 4. The solution of the coupled FHN PDE/LBM model for different coupling mechanisms after 30000 time steps. Shown on the left is the activator density $\rho^{ac}(x, 30)$. In the right panel, we compare the corresponding errors to the difference between the PDE and LBM density computed on the full domain. The latter is marked by the label “steady”.

or constrained runs coupling is much smaller. Clearly, neglecting first order contributions in the coupling scheme is not a good option.

Next, we look at the long term effects of this interfacial error. In Fig. 4, we show the solution after 30000 time steps. The left panel shows that the error of the zeroth order coupling has now propagated over the domain and shifted the solution globally to the right. In fact, all coupled models converge towards a steady state that is different from the steady state obtained with one model on the full domain.

The right panel shows that the modeling errors as a result of the coupling with first order and constrained runs are comparable to the modeling error between the LBM and PDE solution computed on the full domain. These errors are most pronounced in the region where the solution varies strongly (cf. Sect. 2.3). Note that we compared to the PDE steady state reference solution on the full domain here, as we chose to solve predominately with the LBM in the coupled model.

From the numerical experiments, we can also learn something about the relation between the error and the spatial derivatives of the solution at the interface. The (small) interfacial error in Fig. 3 for the coupling with both first order perturbations or the constrained runs scheme comes from the second order term $f_1^{[2]}(x_{pde}, t)$ (18) that is neglected in the computation of the distribution function at the interface. This term is related to the second spatial derivative $\partial^2 \rho(x_{pde}, t) / \partial x^2$ of the solution at the interface (see (22)). Since this second derivate is nonzero at the interface for our FHN example, we observe a local interfacial error.

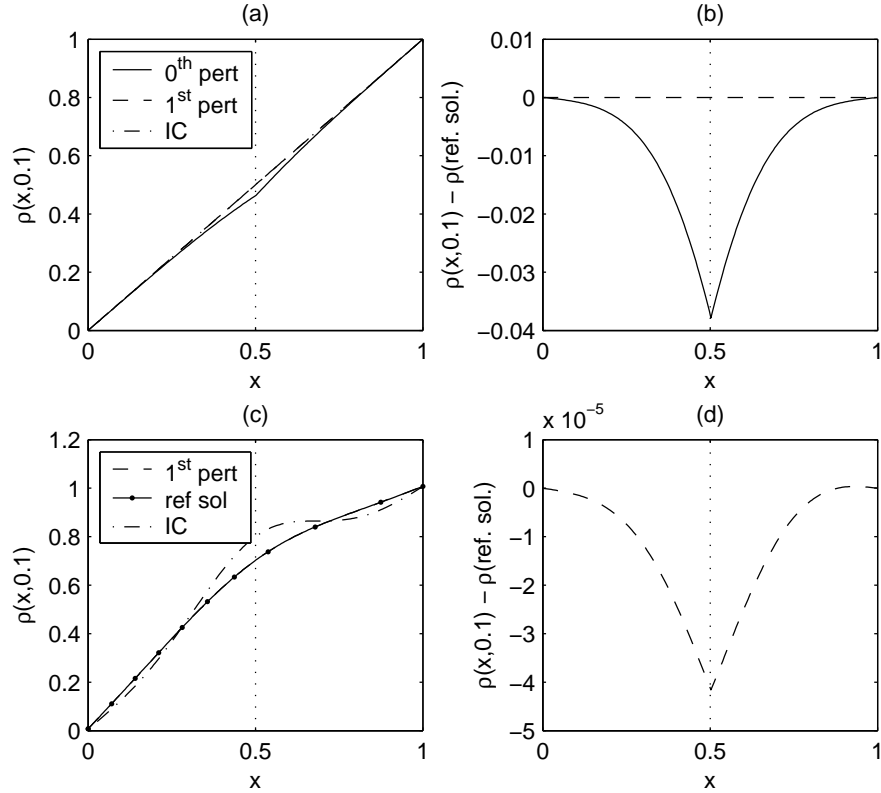


Fig. 5. Illustration on how the error depends on the spatial derivatives of the solution. The example is a pure diffusion system with Dirichlet boundary conditions on the domain $[0, 1]$ for two types of initial conditions. The coupled PDE/LBM system is simulated for 10000 time steps. The position of the interface is marked by a dotted line. Figures (a) and (b) show the solution and the error when the initial condition is a straight line connecting the two boundary conditions. Figures (c) and (d) show respectively the reference solution and solution with first order coupling and the corresponding error for an initial profile with nonzero second derivatives. First order coupling is correct for a solution with only first derivatives, but has a small error when the solution has a nonzero second derivative.

In Fig. 5 we perform an experiment to illustrate this relation. Here, we consider a pure diffusion model problem with Dirichlet boundary conditions $\rho(0, t) = 0$ and $\rho(1, t) = 1$. The domain $[0, 1]$ is discretized with 200 lattice points and the parameters are chosen as $D = 0.2$ and $\Delta t = 0.00001$. The interface is located at $x = 0.5$. The steady state solution is a straight line connecting the density values at the boundary. We simulate the coupled system for 10000 time steps. We impose two different initial conditions: the steady state solution (Fig. 5 (a)-(b)) or an initial condition with a nonzero second

derivative (Fig. 5 (c)-(d)). In the first case, Fig. 5 (b) shows that the error is zero when first order coupling is used, since $\partial^2 \rho / \partial x^2 = 0$ here. In the second case, the solution at $t = 10000 \Delta t$ has a nonzero second derivative and the first order coupling error behaves similar to the error of the zeroth order coupling in Fig. 5 (b). Note the different scale of Fig. 5 (b) and (d).

Of course, when simulating the system in Fig. 5 (c)-(d) for long enough time, the interfacial error for the first order coupling will become zero since the solution converges to the steady state as in Fig. 5 (a)-(b). For the FHN example however, the steady state has a nonzero second derivative at the interface and both the local interfacial error and the resulting global modeling error evolve to a constant nonzero value.

Figures 3 and 4 suggest that the coupling with constrained runs is more accurate than coupling with first order perturbations. This can be explained by comparing (27) to (22). We see that the part corresponding to the reaction term in (22) is approximated correctly by (27) while it does not appear in the first order coupling scheme. At least for our example, this results in a higher accuracy for the constrained runs coupling.

5.3 Spatial Coupling of a Growth-Diffusion PDE and LBM

In this section, we will spatially couple the LBM (23) and the finite difference discretization of the corresponding PDE (24) for the growth-diffusion system from Sect. 2.4. The setup on the one-dimensional domain is described in Fig. 2. We used the D1Q3 scheme and a reaction matrix

$$A = [A_{ij}] = \begin{bmatrix} -R & 0 & 0 \\ 1.1R & 0 & 1.1R \\ 0 & 0 & -R \end{bmatrix} \quad (35)$$

with $R = 0.02$. The relaxation parameter is $\omega = 1.6160$. This LBM leads to a macroscopic growth-diffusion problem (24) with $D = 0.1856$ and $\alpha = 1.315 \cdot 10^{-3}$. Grid parameters are $\Delta x = 1/399$ and $\Delta t = 2.5 \cdot 10^{-6}$. The interface is positioned at $x = 0.25$.

Instead of using the analytical slaving relations derived through a tedious Chapman-Enskog expansion [18], we will use the constrained runs scheme to derive the distributions at the interface numerically, given the density value. Although we only proved stability and convergence of the constrained runs scheme for the BGK LBM with density dependent reaction term (6) in [17] (see Sect. 3), we expect that the scheme can be applied more generally also.

Figure 6 shows the density profile $\rho(x, t)$ and corresponding error of the coupled PDE/LBM model for the growth-diffusion system from Sect. 2.4. As explained in Sect. 5.2, an interfacial error exists because the solution has a nonzero second derivative at the interface. Since the solution grows over time, the error grows as well.

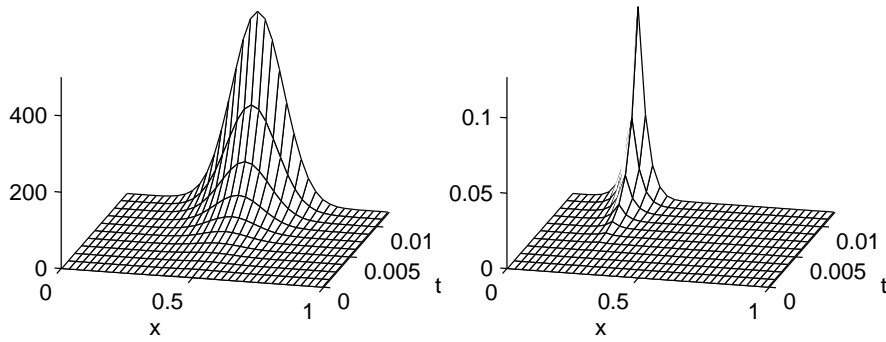


Fig. 6. The solution of the coupled PDE/LBM model for the growth-diffusion system from Sect. 2.4 as a function of space and time. The left panel shows the density $\rho(x,t)$ while the right panel shows the corresponding absolute error. We used constrained runs at the interface, which is positioned at $x = 0.25$.

6 Conclusions and Future Work

In this article, we have studied the coupling of a lattice Boltzmann model (LBM) and a partial differential equation (PDE) describing the same diffusive system, each on a part of a one-dimensional domain. We discretized the PDE using finite differences.

At the interface between the two models, we have a one-to-many problem: the PDE variables (here density) have to be mapped to more LBM variables (the distribution functions). We showed that this can be done both analytically, using results from the Chapman-Enskog expansion, or numerically, using the constrained runs scheme [8, 7]. We use the results from [17], where it is shown that this scheme applied to the LBM under discussion approximates the results from the Chapman-Enskog expansion correctly up to first order. We illustrate these concepts for several diffusive systems.

We show that the solutions of the coupled model are comparable in accuracy to the solution of either the PDE or LBM model on the full domain. We also show that the error made at the interface is proportional to the second derivative of the solution at the interface. The latter is related to the error term for the constrained runs scheme and to the second order term in the Chapman-Enskog expansion.

For certain classes of problems, the current approach is not sufficient and coupling that is correct to higher order is required. In this case, higher order terms in the Chapman-Enskog expansion could be used if these analytic expressions are available. If these are not available, constrained run schemes as proposed in [7] in the context of ODEs, could be useful.

In the current discussion, we used the same space and time step Δx and Δt for both the PDE and LBM sublattice. The focus was on the details of the coupling and how information is exchanged between the two sublattices. The

use of different Δx and Δt values in both regions, optimized to local stability properties, would be a further development. When e.g. the time step of the PDE is a multiple of the LBM time step, interpolation of densities between two PDE time steps is then required to provide the necessary information to the LBM region.

We foresee several applications of a coupled PDE/LBM simulation approach. One example is plasma physics where detailed reaction rates in localized regions determine the macroscopic behavior. Here, the system has a solution that varies rapidly in a localized region of the domain but behaves smoothly in the remainder. In the former region, the approximations made to derive a PDE model will break down and the LBM with the complete reaction details has to be used. In the smooth region, in contrast, the PDE approximations are valid. It is important that the interface is situated in a region where the solution is still slowly varying such that the slaving relations from the Chapman-Enskog expansion hold.

Acknowledgements

The work of P. Van Leemput is supported by project G.0130.03 funded by the Fund for Scientific Research - Flanders and by the Belgian Programme on Interuniversity Attraction Poles, initiated by the Belgian Federal Science Policy Office. The work of W. Vanroose is supported by a DWTC return grant from the Belgian Federal Science Policy Office.

References

1. P. Albuquerque, D. Alemani, B. Chopard, and P. Leone. Coupling a lattice Boltzmann and a finite difference scheme. In M. Bubak, G. D. van Albada, P. M. Sloot, and J. Dongarra, editors, *International Conference on Computational Science - ICCS 2004*, volume 3039 of *Lecture Notes in Computer Science*, pages 540–547. Springer-Verlag, 2004.
2. F. J. Alexander, A. L. Garcia, and D. M. Tartakovsky. Algorithm refinement for stochastic partial differential equations: I. Linear diffusion. *Journal of Computational Physics*, 182:47–66, 2002.
3. B. Chopard, A. Dupuis, A. Masselot, and P. Luthi. Cellular automata and lattice Boltzmann techniques: An approach to model and simulate complex systems. *Advances in Complex Systems*, 5(2/3):103–246, 2002.
4. D. Dab, J.-P. Boon, and Y.-X. Li. Lattice-gas automata for coupled reaction-diffusion equations. *Physical Review Letters*, 66(19):2535–2538, 1991.
5. S. P. Dawson, S. Chen, and G. D. Doolen. Lattice Boltzmann computations for reaction-diffusion equations. *Journal of Chemical Physics*, 98(2):1514–1523, 1993.
6. A. L. Garcia, J. B. Bell, W. Y. Crutchfield, and B. J. Alder. Adaptive mesh and algorithm refinement using direct simulation Monte Carlo. *Journal of Computational Physics*, 154:134–155, 1999.

7. C. W. Gear, T. J. Kaper, I. G. Kevrekidis, and A. Zagaris. Projecting to a slow manifold: Singularly perturbed systems and legacy codes. *SIAM Journal on Applied Dynamical Systems*, 4(3):711–732, 2005.
8. C. W. Gear and I. G. Kevrekidis. Constraint-defined manifolds: A legacy code approach to low-dimensional computation. *Journal of Scientific Computing*, 25(1):17–28, 2005. can also be obtained from arXiv e-Print archive as physics/0312094.
9. I. Ginzbourg and P. M. Adler. Boundary flow condition analysis for the three-dimensional lattice Boltzmann model. *Journal of Physics II France*, 4:191–214, 1994.
10. N. G. Hadjiconstantinou. Hybrid atomistic-continuum formulations and the moving contact-line problem. *Journal of Computational Physics*, 154:245–265, 1999.
11. P. Le Tallec and F. Mallinger. Coupling Boltzmann and Navier-Stokes equations by half fluxes. *Journal of Computational Physics*, 136:51–67, 1997.
12. P. Le Tallec and M. D. Tidriri. Convergence analysis of domain decomposition algorithms with full overlapping for the advection-diffusion problems. *Mathematics of Computation*, 68(226):585–606, 1999.
13. Y. H. Qian, D. D’Humières, and P. Lallemand. Lattice BGK models for Navier-Stokes equation. *Europhysics Letters*, 17(6):479–484, 1992.
14. Y. H. Qian and S. A. Orszag. Scalings in diffusion-driven reaction $A + B \rightarrow C$: Numerical simulations by lattice BGK models. *Journal of Statistical Physics*, 81(1/2):237–253, 1995.
15. S. Tiwari and A. Klar. An adaptive domain decomposition procedure for Boltzmann and Euler equations. *Journal of Computational and Applied Mathematics*, 90:223–237, 1998.
16. P. Van Leemput, K. Lust, and I. G. Kevrekidis. Coarse-grained numerical bifurcation analysis of lattice Boltzmann models. *Physica D: Nonlinear Phenomena*, 210(1–2):58–76, October 2005.
17. P. Van Leemput, W. Vanroose, and D. Roose. Initialization of a lattice Boltzmann model with constrained runs. Technical Report TW 444, Katholieke Universiteit Leuven, Department of Computer Science, December 2005. submitted to *Journal of Computational Physics*.
18. W. Vanroose. Analysis of a lattice Boltzmann model for planar streamer fronts. in preparation, 2006.